International Journal of Thermophysics, Vol. 28, No. 5, October 2007 (© 2007)
DOI: 10.1007/s10765-006-0143-1

Multi-scale Modeling of Radiation Heat Transfer through Nanoporous Superinsulating Materials[1]

Franck Enguehard[2]

In this contribution, the extraordinarily high level of thermal insulation produced by nanoporous materials, which can achieve thermal conductivities down to a few $mW \cdot m^{-1} \cdot K^{-1}$ when they are evacuated to a primary vacuum, is highlighted. The objective here is to quantify the level of radiation heat transfer traveling through a nanoporous material in relation with its composition. The model used here is based on the "non-gray anisotropically scattering Rosseland approximation," which allows the definition of a "radiation thermal conductivity" expressed as a function of the optical properties (complex optical index spectra), mean sizes and volume fractions of the different populations of particles constituting the material. With the help of this simple model, one can draw interesting conclusions concerning the impacts of different parameters related to the microstructure of the nanoporous material on the amplitude of the radiation heat transfer. In the future, this model should help to orient the formulation of new nanoporous materials with optimized radiative properties.

KEY WORDS: Mie theory; nanoporous materials; radiation heat transfer; radiative homogenization.

1. INTRODUCTION

Nanoporous superinsulating materials (NSMs) are the subject of increasing interest for various applications (particularly in the aerospace and construction industries) due to their extraordinary power of thermal insulation [1–5]: whereas air (generally regarded as an excellent thermal

[1] Paper presented at the Seventeenth European Conference on Thermophysical Properties, September 5–8, 2005, Bratislava, Slovak Republic.

[2] CEA/Le Ripault, BP 16, 37260 Monts, France. E-mail: franck.enguehard@cea.fr

insulator) has a thermal conductivity of $25\,\mathrm{mW \cdot m^{-1} \cdot K^{-1}}$ at ambient temperature and pressure, this thermal conductivity falls down to a few $\mathrm{mW \cdot m^{-1} \cdot K^{-1}}$ for an NSM evacuated to a primary vacuum.

Such a level of thermal insulation achieved by NSMs finds its explanation in the microstructure of these materials. Very porous (their porosity is of the order of 90%) and made of extremely fragmented solid matter (the main population of solid constituents is generally brought down to a nanometric scale), they force the conduction heat flux to travel through very tortuous routes consisting of a multitude of elementary thermal resistances located at the coalescences of neighboring nanoparticles. Furthermore, these materials include very small quantities of micrometric scale particles and fibers. Whereas it is generally accepted that the role of the fibers is essentially to provide mechanical reinforcement to the nanoporous structure, on the other hand the presence of the micrometric scale particles is to be related to the level of thermal radiation heat transfer traveling within the NSM. If adequately designed to provide opacity "at the right places in the infrared (IR) spectrum," this microparticle population can quite efficiently cut down the radiation heat flux in the course of its progression within the nanoporous structure.

In this contribution, we wish (i) to develop a model that can be used to quantify the level of radiation heat transfer traveling through an NSM in relation with the composition (sizes, volume fractions, and physical natures of the different populations of constituents) of the material, and then (ii) to exploit this model for the determination of the characteristics (size, volume fraction, and optical properties) of the ideal microparticle population that will produce a maximum opacity "at the right places in the IR spectrum," *i.e.*, a minimum radiation heat flux through the nanoporous structure. To this purpose, we will proceed as follows. First, we will describe in more detail the microstructure of a typical NSM, and we will introduce an idealized, extremely simplified version of this material for our calculations. Then, we will present our thermal radiation model based on the "non-gray anisotropically scattering Rosseland approximation". As a third step, we will use our model for calculation of the transparent spectral bands of an NSM without microparticles, and we will discuss the different interaction phenomena that can possibly take place between the IR wavelengths and the microparticle population. Finally, studies concerning (i) the microparticle volume fraction necessary for a sufficient opacity of the NSM and (ii) a possible optimum size for the microparticle population will be presented.

2. DESCRIPTION OF THE MICROSTRUCTURE OF A TYPICAL NSM AND INTRODUCTION OF A SIMPLIFIED VERSION OF THIS MATERIAL

As introduced previously, an NSM is typically made of (i) nanometric scale particles joined to one another to form a nanoporous matrix, the ultradominant constituent of the material in terms of volume fraction (near 100%), (ii) a small volume fraction (of the order of 1%) of micrometric scale particles expected to provide IR opacity to the NSM, and (iii) a small volume fraction (of the order of 1%) of micrometric scale fibers for reinforcement of the nanoporous structure. In this paper, we will ignore the existence of the fiber population: this population being essentially associated with a mechanical function, we will assume that it does not dramatically impact the radiative properties of the NSM.

The nanoparticles constituting the nanoporous matrix form the dominant population in terms of solid volume fraction (of the order of 5 to 10%); therefore, they must be made of a material that is a good thermal insulator. In a large majority of cases, this material is chosen to be amorphous silicon oxide a-SiO_2.

Figure 1 is a TEM image at a micrometric scale (the surface covered by this image is approximately $8\,\mu m \times 10\,\mu m$) of a particular NSM made of a nanoporous a-SiO_2 matrix and of crystalline silicon carbide SiC microparticles; the nanoporous matrix appears as the gray phase, whereas the SiC microparticles are the dark inclusions.

The nanoporous matrix is extremely porous (its porosity is more than 90%), and a TEM observation focused on this matrix reveals its nanotexture, as shown in Fig. 2. This image being at a scale of the order of 100 nm (the surface covered by the image is approximately $500\,nm \times 650\,nm$), stacks of coalesced a-SiO_2 nanoparticles now appear (dark structures) as well as the three-dimensional (3-D) nanoarchitecture that they constitute. A further TEM analysis focused on one nanoparticle stack allows an approximate evaluation of the average diameter of these a-SiO_2 particles: between 10 and 20 nm.

Pretending to develop a radiative heat transfer model within the NSM that respects the chaotic 3-D nanostructure of the a-SiO_2 matrix appears to be quite unrealistic. As a consequence, we will greatly reduce the complexity of the problem to be solved by simply ignoring the nanostructure of the matrix; we will separate the elementary bricks constituting the matrix, i.e., the a-SiO_2 nanoparticles, from one another and disperse this nanoparticle population randomly in space. In other words, the real NSM presenting a structured nanoporous matrix will from now on be replaced in our calculations by a virtual material presumed radiatively equivalent

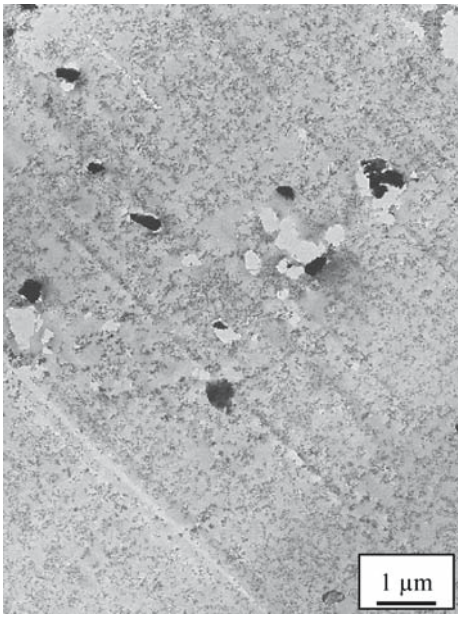

Fig. 1. TEM image of a particular NSM made of a nanoporous a-SiO_2 matrix and of crystalline SiC microparticles. The nanoporous matrix appears as the gray phase, whereas the SiC microparticles are the dark inclusions. The white zones as well as the parallel scratches apparent on this image are due to polishing imperfections.

to the NSM and consisting of the following two particle populations: (i) a population of a-SiO_2 nanoparticles characterized by an average diameter of 10 nm and a volume fraction of 10% and (ii) a population of microparticles the characteristics of which (material, average diameter, and volume fraction) are to be determined.

3. "NON-GRAY ANISOTROPICALLY SCATTERING ROSSELAND APPROXIMATION" BASED THERMAL RADIATION MODEL

3.1. Notion of Radiation Thermal Conductivity

The objective of the work presented here being essentially to compare material solutions and to derive directions towards enhanced thermal insulation efficiencies of NSMs, the notion of radiation thermal conductivity, based on the Rosseland diffusion approximation, appears to be quite convenient.

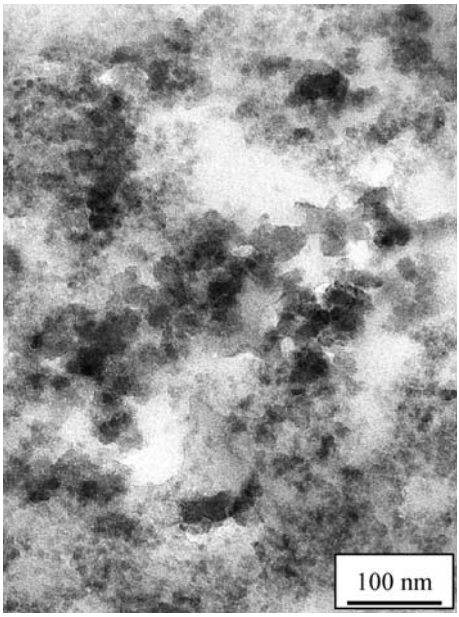

Fig. 2. TEM image of the nanoporous a-SiO_2 matrix appearing in Fig. 1.

The Rosseland diffusion approximation applies when (i) the sample is optically thick and (ii) the scattering phenomenon within the material is isotropic. Under these two circumstances, the radiative flux $\vec{\varphi}^R$ traversing the sample can be expressed in the following form [6]:

$$\vec{\varphi}^R = -\left[\frac{4\pi}{3}\int_0^\infty \frac{1}{\beta_\nu}\frac{d\left(n_\nu^2 L_\nu^0(T)\right)}{dT}d\nu\right]\vec{\nabla}T \tag{1}$$

in which ν is the optical frequency, β_ν is the extinction coefficient spectrum of the material, n_ν is its refractive index spectrum, T is the temperature, and $L_\nu^0(T)$ is the spectral blackbody emissive power distribution (commonly known as Planck's law) at temperature T. The structure of Eq. (1), very similar to Fourier's law of conduction, leads to the introduction of a "radiation thermal conductivity" $k^R(T)$ function of temperature T and expressed as

$$k^R(T) = \frac{4\pi}{3}\int_0^\infty \frac{1}{\beta_\nu}\frac{d\left(n_\nu^2 L_\nu^0(T)\right)}{dT}d\nu \tag{2}$$

When the material is gray, Eq. (2) simplifies greatly and becomes

$$k^R(T) = \frac{16n^2\sigma T^3}{3\beta} \tag{3}$$

where σ is the Stefan-Boltzmann constant (5.67×10^{-8} $\mathrm{W \cdot m^{-2} \cdot K^{-4}}$). For the case of a non-gray material (which is the case of our NSMs), the general expression, Eq. (2), of $k^R(T)$ can be rewritten in the following manner:

$$k^R(T) = \frac{16\sigma T^3}{3}\left\langle \frac{n^2}{\beta} \right\rangle \quad \text{with} \quad \left\langle \frac{n^2}{\beta} \right\rangle = \frac{\displaystyle\int_0^\infty \frac{n_\lambda^2}{\beta_\lambda} \frac{\lambda^{-6}\exp\left(\frac{C_2}{\lambda T}\right)}{\left[\exp\left(\frac{C_2}{\lambda T}\right)-1\right]^2} d\lambda}{\displaystyle\int_0^\infty \frac{\lambda^{-6}\exp\left(\frac{C_2}{\lambda T}\right)}{\left[\exp\left(\frac{C_2}{\lambda T}\right)-1\right]^2} d\lambda} \tag{4}$$

where λ is the wavelength and C_2 is the second constant of Planck's law (14388 $\mu\mathrm{m \cdot K}$). Comparing Eqs. (3) and (4) of the radiation thermal conductivity for a gray and a non-gray material, one notices that the quantity n^2/β, independent of the wavelength for a gray material, is replaced by an average value of the $n_\lambda^2/\beta_\lambda$ spectrum, noted $\langle n^2/\beta \rangle$ in Eq. (4) for a non-gray material. The weight function $\omega_T(\lambda)$ on which the calculation of the average value $\langle n^2/\beta \rangle$ is based has the following form:

$$\omega_T(\lambda) = \frac{\lambda^{-6}\exp\left(\frac{C_2}{\lambda T}\right)}{\left[\exp\left(\frac{C_2}{\lambda T}\right)-1\right]^2} \tag{5}$$

As mentioned previously, the Rosseland diffusion approximation applies when the scattering phenomenon within the material can be considered to be isotropic. This condition may not be fulfilled with our NSMs, the microparticles that they contain having sizes of the same order of magnitude as the IR wavelengths. To circumvent this difficulty, Chu et al. [7] recommended replacement of the β_λ spectrum appearing in Eq. (4) of $k^R(T)$ by an effective extinction coefficient spectrum β_λ^e defined by

$$\beta_\lambda^e = \beta_\lambda - g_\lambda \sigma_\lambda \tag{6}$$

where g_λ and σ_λ are the asymmetry factor and scattering coefficient spectra of the material. As a consequence, the evaluations that we will make

throughout this paper of the radiation thermal conductivities $k^R(T)$ of our NSMs will be based on the following formula:

$$k^R(T) = \frac{16\sigma T^3}{3} \frac{\int_0^\infty \omega_T(\lambda) \frac{n_\lambda^2}{\beta_\lambda^e} d\lambda}{\int_0^\infty \omega_T(\lambda) d\lambda} \tag{7}$$

3.2. Optical and Radiative Homogenization of an NSM

To perform a $k^R(T)$ evaluation as described above, one needs the refractive index (n_λ) as well as the effective extinction coefficient (β_λ^e) spectra of the NSM under study. For the general case of an NSM made of several populations of randomly distributed particles superimposed in air, each population of particles brings its own optical (complex optical index spectrum of the material constituting the particles) and radiative (effective extinction coefficient spectrum of the population) characteristics to the ensemble, and the calculation of the optical and radiative characteristics of the NSM must rely on these inputs.

We perform the optical homogenization of our NSMs *via* Rayleigh's extended rule of mixtures [8]. Applied to relative dielectric permittivities ε_λ defined by $\varepsilon_\lambda = (n_\lambda - jk_\lambda)^2$ where n_λ and k_λ are the refractive and extinction indices, this rule yields

$$\frac{\varepsilon_\lambda^m - \varepsilon_\lambda^h}{\varepsilon_\lambda^m + 2\varepsilon_\lambda^h} = \sum_i f_i \frac{\varepsilon_\lambda^i - \varepsilon_\lambda^h}{\varepsilon_\lambda^i + 2\varepsilon_\lambda^h} \tag{8}$$

where (i) the superscripts m, h, and i indicate quantities referring to the mixture, to the host material, and to the different populations of inclusions, respectively, and (ii) the f_i's are the volume fractions of the different populations of inclusions.

For the case of our NSMs, the host material is air (with dielectric permittivity ε_λ^h equal to 1), and two populations of particles are to be considered: on the one hand the a-SiO_2 nanoparticle population, and on the other hand the microparticle population. Under these circumstances, transforming Eq. (8) yields the following expression for the relative dielectric permittivity ε_λ of the NSM:

$$\varepsilon_\lambda = \frac{\Pi + \frac{3f^{\mathrm{np}}\varepsilon_\lambda^{\mathrm{np}}}{2+\varepsilon_\lambda^{\mathrm{np}}} + \frac{3f^{\mu\mathrm{p}}\varepsilon_\lambda^{\mu\mathrm{p}}}{2+\varepsilon_\lambda^{\mu\mathrm{p}}}}{\Pi + \frac{3f^{\mathrm{np}}}{2+\varepsilon_\lambda^{\mathrm{np}}} + \frac{3f^{\mu\mathrm{p}}}{2+\varepsilon_\lambda^{\mu\mathrm{p}}}} \tag{9}$$

In this formula, the superscripts np and μp refer to the nanoparticle and microparticle populations, respectively, and Π, f^{np}, and $f^{\mu\mathrm{p}}$ are the porosity of the NSM and the nanoparticle and microparticle volume fractions within the material (these three quantities verifying $\Pi + f^{\mathrm{np}} + f^{\mu\mathrm{p}} = 1$). Eq. (9) allows calculation of the ε_λ spectrum of the NSM, and subsequently its n_λ spectrum through the relation $\varepsilon_\lambda = (n_\lambda - jk_\lambda)^2$.

Our procedure for the radiative homogenization of our NSMs relies on the principle of addition of cross-sections. An effective extinction coefficient being regarded as an effective extinction cross-section per unit volume, this quantity is cumulative, so that the effective extinction coefficient spectrum β_λ^e of an NSM can be evaluated simply by addition of the β_λ^e spectra related to the nanoparticle and microparticle populations constituting the material:

$$\beta_\lambda^e = \beta_\lambda^{\mathrm{e-np}} + \beta_\lambda^{\mathrm{e}-\mu\mathrm{p}} \tag{10}$$

with the obvious notations introduced previously.

3.3. Determination of the Optical and Radiative Properties of the Nanoparticle and Microparticle Populations

The optical properties of the two particle populations (*i.e.*, the complex optical index spectra of the two materials constituting these two populations) are taken from Ref. 9.

The process of evaluation of the radiative properties of the two particle populations (*i.e.*, the two effective extinction coefficient spectra $\beta_\lambda^{\mathrm{e-np}}$ and $\beta_\lambda^{\mathrm{e}-\mu\mathrm{p}}$ related to these two populations) consists of several steps. First, we resort to the Mie theory, which accounts for the interaction of a monochromatic electromagnetic wave with a single solid particle. Mie formulae for a particle of spherical shape are given in Ref. 6. The inputs of this calculation are, on the one hand, the size parameter x_λ defined by $x_\lambda = \pi d/\lambda$ where d and λ are the particle diameter and the irradiation wavelength, respectively, and, on the other hand, the complex optical index $n_\lambda - jk_\lambda$ of the material constituting the particle at the irradiation wavelength λ. Application of the formulae of the Mie theory leads to the evaluation of several quantities: on the one hand, the spectral absorption, scattering and extinction cross-sections (respectively, s_λ^{abs}, s_λ^{sca}, and s_λ^{ext}, with obvious notations) produced by the particle (these three cross-sections verifying $s_\lambda^{\mathrm{abs}} + s_\lambda^{\mathrm{sca}} = s_\lambda^{\mathrm{ext}}$), and, on the other hand, the spectral scattering phase function $\Phi_\lambda(\theta)$ and the associated spectral asymmetry factor g_λ.

As a second step, based on the characteristics of the interaction of the monochromatic electromagnetic wave with a single particle (results

obtained above), we proceed to the calculation of the cross-sections, the phase function, and the asymmetry factor when the interaction is no more with a single particle but with a population of particles of volume fraction f. If the particles constituting the population are of uniform size (assumption that we make throughout this paper for all the particle populations that we deal with), it is known [6] that the spectral scattering phase function $\Phi_\lambda(\theta)$ and hence the associated spectral asymmetry factor g_λ are unchanged when referring either to a single particle or to a whole population. Concerning the spectral absorption, scattering, and extinction cross-sections (respectively, S_λ^{abs}, S_λ^{sca}, and S_λ^{ext}) produced by a volume V occupied by the particle population, a very straightforward calculation based on the principle of summation of cross-sections yields

$$S_\lambda^{\text{abs}} = \frac{6fVs_\lambda^{\text{abs}}}{\pi d^3}, \quad S_\lambda^{\text{sca}} = \frac{6fVs_\lambda^{\text{sca}}}{\pi d^3} \quad \text{and} \quad S_\lambda^{\text{ext}} = \frac{6fVs_\lambda^{\text{ext}}}{\pi d^3} = S_\lambda^{\text{abs}} + S_\lambda^{\text{sca}} \tag{11}$$

so that the spectral absorption, scattering, and extinction coefficients (respectively, κ_λ, σ_λ, and β_λ) produced by the particle population, defined as the related cumulative cross-sections per unit volume, have the following expressions:

$$\kappa_\lambda = \frac{S_\lambda^{\text{abs}}}{V} = \frac{6fs_\lambda^{\text{abs}}}{\pi d^3}, \quad \sigma_\lambda = \frac{S_\lambda^{\text{sca}}}{V} = \frac{6fs_\lambda^{\text{sca}}}{\pi d^3} \quad \text{and} \quad \beta_\lambda = \frac{S_\lambda^{\text{ext}}}{V} = \frac{6fs_\lambda^{\text{ext}}}{\pi d^3} = \kappa_\lambda + \sigma_\lambda \tag{12}$$

In the preceding developments the principle of summation of cross-sections is assumed to be valid, which may not be the case especially when the volume fraction f of the particle population is important. Here the phenomenon of dependent scattering has to be taken into consideration; this phenomenon leads to a decrease in the scattering efficiency [10] and a simultaneous increase in the absorption efficiency. These tendencies are integrated in our model *via* very simple correction terms that have been validated (either theoretically or experimentally) over the volume fraction domain $f < 0.1$ [11]. Eqs. (12) are replaced by

$$\kappa_\lambda = \frac{6fs_\lambda^{\text{abs}}}{\pi d^3}\frac{(1+2f)^2}{(1-f)^4}, \quad \sigma_\lambda = \frac{6fs_\lambda^{\text{sca}}}{\pi d^3}\frac{(1-f)^4}{(1+2f)^2} \quad \text{and} \quad \beta_\lambda = \kappa_\lambda + \sigma_\lambda \tag{13}$$

3.4. Summary of our Procedure for the Evaluation of the Radiation Thermal Conductivities of our NSMs

The NSM under study is supposed to be made (i) of a population of a-SiO_2 nanoparticles characterized by a complex optical index spectrum $n_\lambda^{\text{np}} - jk_\lambda^{\text{np}}$ equal to the spectrum of a-SiO_2, a uniform diameter

$d^{np} = 10\,\text{nm}$, and a volume fraction $f^{np} = 10\%$, and (ii) of a population of microparticles characterized by a complex optical index spectrum $n_\lambda^{\mu p} - jk_\lambda^{\mu p}$, a uniform diameter $d^{\mu p}$, and a volume fraction $f^{\mu p}$.

The determination of the refractive index spectrum n_λ of the NSM is performed in three steps: (i) evaluation of the relative dielectric permittivity spectra of the two materials constituting the two populations *via* the formulae $\varepsilon_\lambda^{np} = \left(n_\lambda^{np} - jk_\lambda^{np}\right)^2$ and $\varepsilon_\lambda^{\mu p} = \left(n_\lambda^{\mu p} - jk_\lambda^{\mu p}\right)^2$, (ii) calculation of the relative dielectric permittivity spectrum ε_λ of the NSM using Eq. (9), and (iii) derivation of the refractive index spectrum n_λ of the NSM *via* the relation $n_\lambda = \text{Re}\left(\sqrt{\varepsilon_\lambda}\right)$.

The determination of the effective extinction coefficient spectrum β_λ^e of the NSM is performed in four steps: (i) evaluation *via* the Mie theory of the elementary spectral cross-sections s_λ^{abs-np}, s_λ^{sca-np}, $s_\lambda^{abs-\mu p}$, and $s_\lambda^{sca-\mu p}$ as well as the spectral asymmetry factors g_λ^{np} and $g_\lambda^{\mu p}$ produced by the two populations, (ii) calculation of the absorption and scattering coefficient spectra κ_λ^{np}, σ_λ^{np}, $\kappa_\lambda^{\mu p}$, and $\sigma_\lambda^{\mu p}$ produced by the two populations using Eqs. (13), (iii) derivation of the effective extinction coefficient spectra β_λ^{e-np} and $\beta_\lambda^{e-\mu p}$ of the two populations using the formulae,

$$\beta_\lambda^{e-np} = \kappa_\lambda^{np} + \left(1 - g_\lambda^{np}\right)\sigma_\lambda^{np} \quad \text{and} \quad \beta_\lambda^{e-\mu p} = \kappa_\lambda^{\mu p} + \left(1 - g_\lambda^{\mu p}\right)\sigma_\lambda^{\mu p}, \quad (14)$$

and (iv) evaluation of the effective extinction coefficient spectrum β_λ^e of the NSM *via* the addition Eq. (10).

Once the n_λ and β_λ^e spectra of the NSM have been determined, the radiation thermal conductivity $k^R(T)$ of the material at a given temperature T is evaluated by numerical integration of Eq. (7).

4. DETERMINATION OF THE CHARACTERISTICS OF THE IDEAL MICROPARTICLE POPULATION

4.1. Extinction Properties of the Nanoporous a-SiO_2 Matrix

In this section, we consider an NSM made of exclusively the a-SiO_2 nanoparticle population (the characteristics of which are recalled here: uniform diameter $d^{np} = 10\,\text{nm}$ and volume fraction $f^{np} = 10\%$).

Before proceeding to the n_λ, β_λ^e, and $k^R(T)$ evaluations as described above, we must determine the spectral interval $[\lambda_1; \lambda_2]$ that is relevant to the calculations. Clearly, the bounds of this interval result from the features of the weight function $\omega_T(\lambda)$ appearing in Eq. (7) of the radiation thermal conductivity $k^R(T)$. This function $\omega_T(\lambda)$ has a shape that is very similar to the one of Planck's law $L_\lambda^0(T)$, and a numerical analysis shows (i) that 1% of the total weight $\int_0^\infty \omega_T(\lambda)d\lambda$ lies within the spectral

interval $\left[0; \frac{1251\mu\mathrm{m}\cdot\mathrm{K}}{T}\right]$, and (ii) that 1% of the total weight $\int_0^\infty \omega_T(\lambda)d\lambda$ lies within the spectral interval $\left[\frac{15967\mu\mathrm{m}\cdot\mathrm{K}}{T}; \infty\right]$. In other words, the spectral interval $\left[\frac{1251\mu\mathrm{m}\cdot\mathrm{K}}{T}; \frac{15967\mu\mathrm{m}\cdot\mathrm{K}}{T}\right]$ contains 98% of the total weight $\int_0^\infty \omega_T(\lambda)d\lambda$ and hence can be regarded as the relevant spectral interval $[\lambda_1(T)\,;\,\lambda_2(T)]$ for the calculations. At room temperature $T = 300$ K, this interval $[\lambda_1(T)\,;\,\lambda_2(T)]$ is approximately $[4\,\mu\mathrm{m}\,;\,54\,\mu\mathrm{m}]$.

The a-SiO_2 nanoparticles being very small compared to the IR wavelengths, the size parameters $x_\lambda^{\mathrm{np}} = \pi d^{\mathrm{np}}/\lambda$ are also very small, and the interaction between the IR wavelengths and the nanoparticle population degenerates into the well-known Rayleigh scattering phenomenon [6]. Under these circumstances, the ultradominant mode of extinction is absorption ($\sigma_\lambda^{\mathrm{np}} << \kappa_\lambda^{\mathrm{np}}$), so that the effective extinction spectrum $\beta_\lambda^{\mathrm{e-np}}$ of the nanoparticle population is equal to its absorption spectrum $\kappa_\lambda^{\mathrm{np}}$ and is in direct relation with the extinction index spectrum k_λ^{np} of a-SiO_2.

The complex optical index spectrum $n_\lambda^{\mathrm{np}} - jk_\lambda^{\mathrm{np}}$ of a-SiO_2 is taken from Ref. 9, and the k_λ^{np} component of this spectrum is reproduced in Fig. 3. In this figure are also plotted two vertical dashed lines indicating the bounds of the relevant spectral interval at room temperature. a-SiO_2 appears to be very transparent ($k_\lambda^{\mathrm{np}} \leqslant 10^{-4}$) for wavelengths between 0.16 and 4.1 μm; this spectral band can then be expected to contribute strongly to the radiation thermal conductivity $k^R(T)$ of the nanoporous a-SiO_2 matrix. On the other hand, this spectral band overlaps very little with the

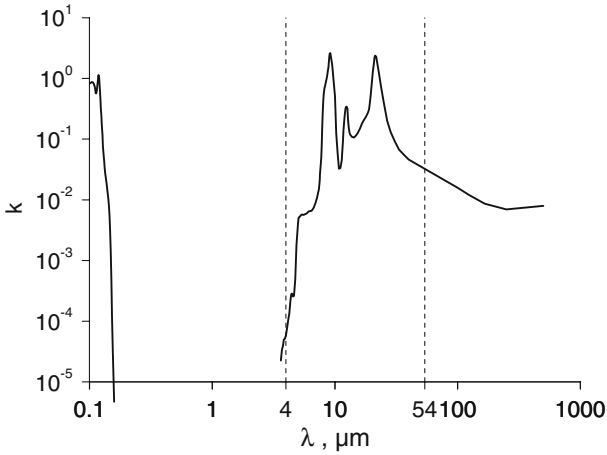

Fig. 3. Extinction index spectrum of a-SiO_2 (taken from Ref. 9).

relevant spectral interval at room temperature (the overlap is limited to $[4\,\mu\text{m}\,;4.1\,\mu\text{m}]$), so that the main contribution to the radiation thermal conductivity $k^R(T)$ of the nanoporous a-SiO_2 matrix at room temperature can be expected to come from a narrow spectral interval centered at $\lambda = 4\,\mu\text{m}$.

As seen previously, the evaluation of the radiation thermal conductivity $k^R(T)$ results from integration over the whole spectrum of the quantity $\omega_T(\lambda)n_\lambda^2/\beta_\lambda^e$ (refer to Eq. (7)). After calculation of the n_λ and β_λ^e spectra of the nanoporous a-SiO_2 matrix through the procedure described in Section 3, one obtains the $\omega_T(\lambda)n_\lambda^2/\beta_\lambda^e$ spectrum (at room temperature) of Fig. 4. This plot confirms that the wavelengths contributing to the radiation thermal conductivity $k^R(T)$ of the nanoporous a-SiO_2 matrix at room temperature are located essentially around $4\,\mu$m: a numerical analysis reveals that 60% of the integral $\int_0^\infty \omega_T(\lambda)\frac{n_\lambda^2}{\beta_\lambda^e}d\lambda$ is provided by the spectral band $[3.4\,\mu\text{m}; 5.6\,\mu\text{m}]$. From this calculation one derives an immediate consequence concerning the microparticle population that is inserted into an NSM in order to cut down its radiation thermal conductivity $k^R(T)$ at room temperature: for an improved efficiency, this microparticle population should be designed to provide a strong extinction around $4\,\mu$m.

The $\omega_T(\lambda)n_\lambda^2/\beta_\lambda^e$ spectrum of Fig. 4 allows numerical evaluation (*via* Eq. (7)) of the radiation thermal conductivity $k^R(T)$ of the nanoporous a-SiO_2 matrix at room temperature: $6.6\ \text{mW}\cdot\text{m}^{-1}\cdot\text{K}^{-1}$. Compared to the

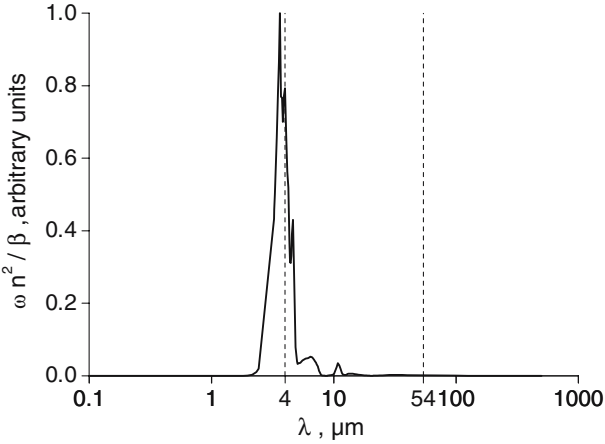

Fig. 4. Calculated $\omega_T(\lambda)n_\lambda^2/\beta_\lambda^e$ spectrum of the nanoporous a-SiO_2 matrix at room temperature.

order of magnitude of the effective thermal conductivity of an NSM related to solid heat conduction (a few $\mathrm{mW \cdot m^{-1} \cdot K^{-1}}$ under primary vacuum), this value of 6.6 $\mathrm{mW \cdot m^{-1} \cdot K^{-1}}$ for the radiation thermal conductivity is quite important and must be reduced by the proper choice of the characteristics (*i.e.*, material, diameter, and volume fraction) of the microparticle population.

4.2. Study of the Interaction Phenomena Between the IR Wavelengths and the Microparticle Population and of Their Impacts on the Radiation Thermal Conductivity of an NSM

As written above, for an improved efficiency of radiative insulation of an NSM, the microparticle population that it contains should be designed to provide a strong extinction around 4 μm. There are two ways to provide extinction: absorption and scattering. In order to decorrelate the impacts of these two extinction modes on the $\omega_T(\lambda) n_\lambda^2 / \beta_\lambda^e$ spectrum of an NSM, we have selected two materials presenting extremely different optical extinction properties around 4 μm: (i) at one extreme, a-SiO_2, very transparent around 4 μm ($k_\lambda = 6 \times 10^{-5}$ at this wavelength), and (ii) at the other extreme, graphite, very opaque around 4 μm ($k_\lambda = 4$ at this wavelength) (the extinction index spectrum of graphite (taken from Ref. 9) is plotted in Fig. 5).

We have calculated the $\omega_T(\lambda) n_\lambda^2 / \beta_\lambda^e$ spectra (at room temperature) of the two NSMs consisting, on the one hand, of the same nanoparticle

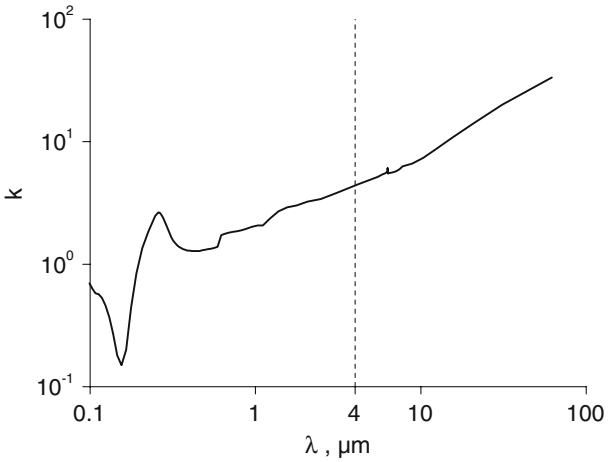

Fig. 5. Extinction index spectrum of graphite (taken from Ref. 9).

population (material a-SiO_2, uniform diameter $d^{np} = 10\,nm$, volume fraction $f^{np} = 10\%$) and, on the other hand, of two microparticle populations (uniform diameter $d^{\mu p} = 1\,\mu m$, volume fraction $f^{\mu p} = 1\%$) differing only by the nature of the material constituting the microparticles (a-SiO_2 or graphite). These two $\omega_T(\lambda)n_\lambda^2/\beta_\lambda^e$ spectra are plotted on the graphs of Figs. 6 and 7 (Fig. 7 is an enlargement of Fig. 6) together with the $\omega_T(\lambda)n_\lambda^2/\beta_\lambda^e$ spectrum of the nanoporous a-SiO_2 matrix (previously exhibited in Fig. 4).

Quite clearly, the addition of microparticles (whatever their nature) to the nanoporous matrix results in significantly reduced values of the $\omega_T(\lambda)n_\lambda^2/\beta_\lambda^e$ spectrum and hence in a significantly lower value of the radiation thermal conductivity $k^R(T)$: whereas this parameter was 6.6 m $W \cdot m^{-1} \cdot K^{-1}$ for the nanoporous a-SiO_2 matrix, it falls to 1.7 m $W \cdot m^{-1} \cdot K^{-1}$ when a-SiO_2 microparticles are incorporated into the matrix, and to 0.7 m$W \cdot m^{-1} \cdot K^{-1}$ when the a-SiO_2 microparticles are replaced by graphite microparticles. The role of the microparticle population within an NSM is therefore clearly demonstrated; whatever its nature, it contributes to cut down the radiation thermal conductivity of the NSM by providing extinction to the ensemble.

For the case of the a-SiO_2 microparticle population, the constitutive material being very transparent for wavelengths under 4 μm, no absorption

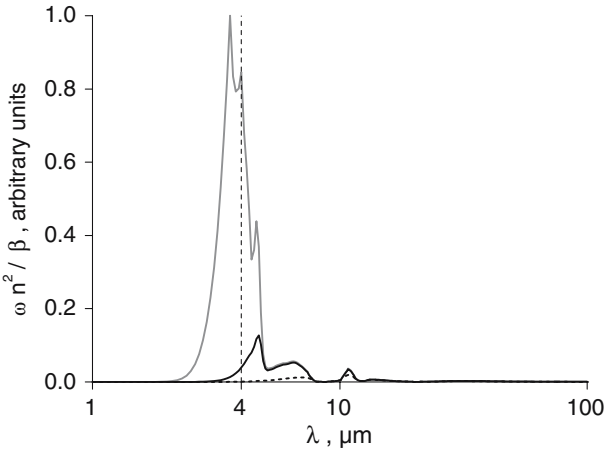

Fig. 6. Calculated $\omega_T(\lambda)n_\lambda^2/\beta_\lambda^e$ spectra (at room temperature) (i) of the NSM containing an a-SiO_2 microparticle population (solid line) and (ii) of the NSM containing a graphite microparticle population (dashed line). The grey solid line represents the $\omega_T(\lambda)n_\lambda^2/\beta_\lambda^e$ spectrum of the nanoporous a-SiO_2 matrix (previously exhibited in Fig. 4).

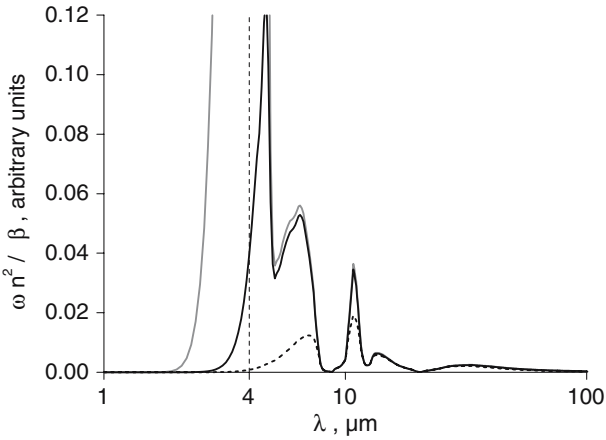

Fig. 7. Enlargement of Fig. 6.

can be expected from this population over this wavelength interval. In order to confirm this point, referring to the expression of the effective extinction coefficient $\beta_\lambda^e = \kappa_\lambda + (1 - g_\lambda)\,\sigma_\lambda$, we have calculated an effective albedo spectrum Ω_λ^e for the a-SiO_2 microparticle population, this spectrum Ω_λ^e being defined by

$$\Omega_\lambda^e = \frac{(1 - g_\lambda)\,\sigma_\lambda}{\beta_\lambda^e} = \frac{(1 - g_\lambda)\,\sigma_\lambda}{\kappa_\lambda + (1 - g_\lambda)\,\sigma_\lambda} \tag{15}$$

The Ω_λ^e spectrum of the a-SiO_2 microparticle population ($d^{\mu p} = 1\,\mu$m and $f^{\mu p} = 1\%$) is plotted on the graph of Fig. 8. The Ω_λ^e values of this population are equal to one for wavelengths under $4\,\mu$m, which proves that the a-SiO_2 microparticle population provides extinction to the NSM over this spectral band exclusively through the scattering phenomenon.

The case of the graphite microparticle population is different in that graphite is strongly absorbing at IR wavelengths. One can then anticipate that this population provides extinction through the superposition of the scattering and absorption phenomena. The Ω_λ^e spectrum of the graphite microparticle population ($d^{\mu p} = 1\,\mu$m and $f^{\mu p} = 1\%$), also plotted on the graph of Fig. 8, confirms this point: around $4\,\mu$m, the effective albedos have values around 0.5, which means that scattering and absorption participate at identical levels to the overall extinction provided by the graphite microparticle population.

Since scattering is the only source of extinction for the a-SiO_2 microparticle population, one expects the level of IR opacity provided by this population to be lower than that provided by the graphite microparticle

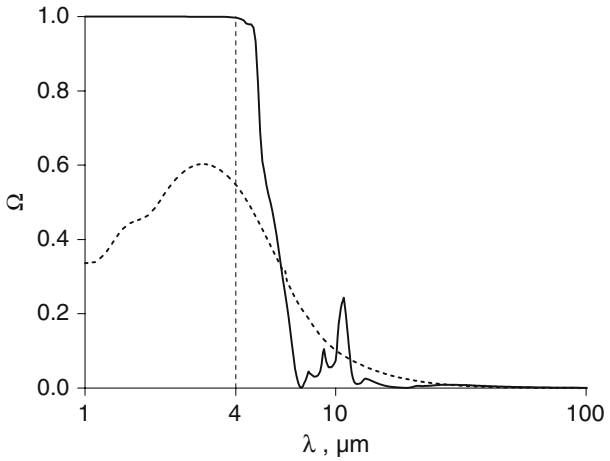

Fig. 8. Effective albedo Ω_λ^e spectra (i) of a-SiO_2 microparticle population ($d^{\mu p} = 1\,\mu$m and $f^{\mu p} = 1\%$) (solid line) and (ii) of a graphite microparticle population (same $d^{\mu p}$ and $f^{\mu p}$) (dashed line).

population, for which absorption also contributes to the overall extinction. The plot of Fig. 9, showing the effective extinction coefficient β_λ^e spectra of the two a-SiO_2 and graphite microparticle populations, corroborates this argument; except over the a-SiO_2 phonon absorption band located between 9 and 21 μm, the β_λ^e values of the graphite population are significantly higher than the ones of the a-SiO_2 population, resulting in a lower value of the radiation thermal conductivity $k^R(T)$ of the NSM when made of the graphite microparticle population. However, it is to be emphasized that, although the addition of absorption to the extinction phenomenon (by the replacement of the a-SiO_2 population by a graphite population) appears to be quite efficient in cutting down the radiation thermal conductivity (this parameter decreases from 1.7 to 0.7 $\mathrm{mW \cdot m^{-1} \cdot K^{-1}}$ when the a-SiO_2 microparticles are replaced by graphite microparticles), the scattering phenomenon itself as a source of extinction is also very productive: the radiation thermal conductivity of the nanoporous a-SiO_2 matrix decreases from 6.6 to 1.7 $\mathrm{mW \cdot m^{-1} \cdot K^{-1}}$ when a-SiO_2 microparticles are incorporated into the matrix.

5. ORDER OF MAGNITUDE OF THE VOLUME FRACTION OF THE MICROPARTICLE POPULATION

The radiation thermal conductivity model described previously can give interesting information concerning the order of magnitude of the

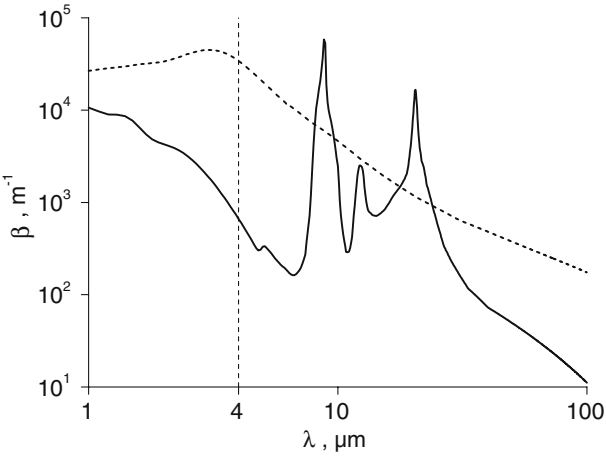

Fig. 9. Effective extinction coefficient β_λ^e spectra (i) of a a-SiO_2 microparticle population ($d^{\mu p} = 1\,\mu$m and $f^{\mu p} = 1\%$) (solid line), and (ii) of a graphite microparticle population (same $d^{\mu p}$ and $f^{\mu p}$) (dashed line).

microparticle population volume fraction that is necessary for an efficient drop in the radiation heat flux through an NSM. In this section, we focus on two particular NSMs made of the same a-SiO_2 nanoparticle population ($d^{np} = 10$ nm and $f^{np} = 10\%$) and of two microparticle populations of identical diameters ($d^{\mu p} = 1\,\mu$m) differing only by the nature of the material constituting the microparticles: a-SiO_2 for NSM1 and graphite for NSM2. The plot of Fig. 10 shows the evolution of the radiation thermal conductivities $k^R(T)$ (at room temperature) of these two NSMs *versus* the microparticle population volume fractions $f^{\mu p}$. This figure clearly indicates that the quantity $k^R(T)$ falls considerably as soon as a tiny microparticle population is inserted into the NSM: a value of the microparticle population volume fraction $f^{\mu p}$ as small as $1‰$ produces a radiation thermal conductivity $k^R(T)$ that is divided by a factor of 2.3 for NSM1 and of 5.6 for NSM2. On the other hand, once this rapid evolution of $k^R(T)$ *versus* $f^{\mu p}$ is completed, the radiation thermal conductivity $k^R(T)$ decreases very slowly with the volume fraction $f^{\mu p}$, so that, based on this behavior of the $f^{\mu p} \mapsto k^R(T)$ curve, it appears counterproductive to incorporate an important volume fraction of microparticles into an NSM: an augmented value of the parameter $f^{\mu p}$ (say a few % instead of a few ‰) will have virtually no impact on the radiation thermal conductivity $k^R(T)$ but on the other hand could possibly affect (*via* the percolation phenomenon) the solid thermal conductivity of the material.

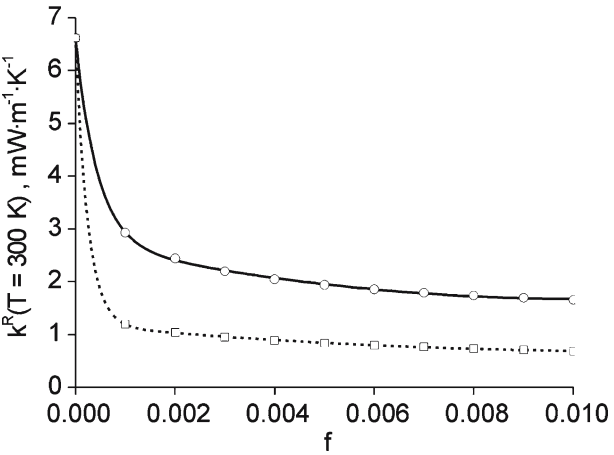

Fig. 10. Dependence of the radiation thermal conductivity $k^R(T)$ of an NSM (at $T = 300\,\mathrm{K}$) as a function of the microparticle population volume fraction $f^{\mu\mathrm{p}}$. Circles and solid curve refer to an NSM made of a a-SiO_2 nanoparticle population ($d^{\mathrm{np}} = 10\,\mathrm{nm}$ and $f^{\mathrm{np}} = 10\%$) and of a a-SiO_2 microparticle population ($d^{\mu\mathrm{p}} = 1\,\mu\mathrm{m}$). Squares and dashed curve refer to an NSM made of the same a-SiO_2 nanoparticle population and of a graphite microparticle population with an unchanged microparticle diameter ($d^{\mu\mathrm{p}} = 1\,\mu\mathrm{m}$). Circles and squares correspond to values produced by our model, and the solid and dashed curves are fits of these two series of data.

6. OPTIMUM SIZE FOR THE MICROPARTICLE POPULATION

As noted earlier, for an improved efficiency of radiative insulation of an NSM, the microparticle population that it contains should be designed to provide a strong extinction around $4\,\mu\mathrm{m}$. If the material constituting this microparticle population is given, its extinction index spectrum and related absorption bands or peaks are also given, and in no way the average diameter $d^{\mu\mathrm{p}}$ of the microparticle population will change the spectral locations of these absorption sources. On the other hand, it is well known that the value of the parameter $d^{\mu\mathrm{p}}$ impacts on the spectral location of the scattering phenomenon, so that it may reasonably be expected that an optimum microparticle population diameter $d^{\mu\mathrm{p}}$ exists for which the scattering phenomenon is positioned exactly over the tracked wavelength of $4\,\mu\mathrm{m}$.

For the purpose of illustration, let us first consider a microparticle population made of graphite and of volume fraction $f^{\mu\mathrm{p}}$ equal to $1‰$.

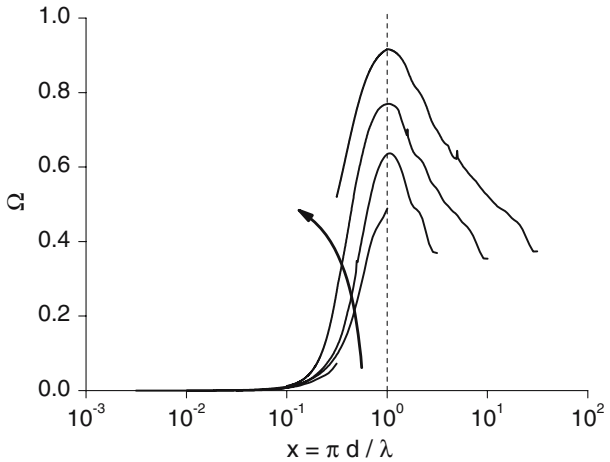

Fig. 11. Effective albedo $\Omega_\lambda^{e-\mu p}$ spectra of five graphite microparticle populations of identical volume fractions ($f^{\mu p} = 1‰$) differing only by the microparticle uniform diameter $d^{\mu p}$ (100 nm, 300 nm, 1 μm, 3 μm, and 10 μm). The five $\Omega_\lambda^{e-\mu p}$ spectra are plotted *versus* the size parameters $x_\lambda^{\mu p} = \pi d^{\mu p}/\lambda$. Arrow on the figure indicates increasing values of $d^{\mu p}$.

For five different values (100 nm, 300 nm, 1 μm, 3 μm, and 10 μm) of the uniform diameter $d^{\mu p}$ of this population (the volume fraction $f^{\mu p}$ being held constant at $1‰$), we have calculated the resulting effective albedo $\Omega_\lambda^{e-\mu p}$ and effective extinction coefficient $\beta_\lambda^{e-\mu p}$ spectra produced by the population. For each value of the diameter $d^{\mu p}$, these two spectra, $\Omega_\lambda^{e-\mu p}$ and $\beta_\lambda^{e-\mu p}$, are plotted *versus* the size parameter $x_\lambda^{\mu p} = \pi d^{\mu p}/\lambda$ on the graphs of Figs. 11 and 12.

The plot of Fig. 11 reveals maxima of the five $\Omega_\lambda^{e-\mu p}$ curves that are all located at $x_\lambda^{\mu p} \approx 1$ (when these maxima appear). This means that, a diameter $d^{\mu p}$ being given for the graphite microparticle population, the fraction of the overall extinction produced by this population through the scattering phenomenon is a maximum at wavelengths λ of the order of $\pi d^{\mu p}$. In the particular case studied here, this increase in the rate of participation of the scattering for $x_\lambda^{\mu p} \approx 1$ comes with an increase in the overall extinction over this size parameter domain, as shown on the graph of Fig. 12: similarly to the curves of Fig. 11, the five effective extinction coefficient $\beta_\lambda^{e-\mu p}$ spectra displayed in Fig. 12 exhibit maxima that are all located at $x_\lambda^{\mu p} \approx 1$ (when these maxima appear). Moreover, for each of the five $\beta_\lambda^{e-\mu p}$ spectra of this plot,

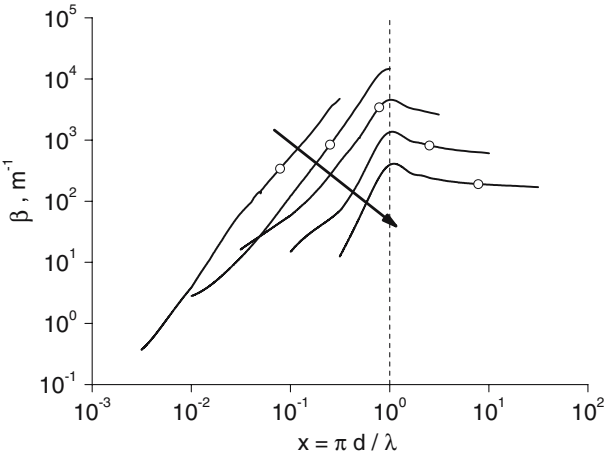

Fig. 12. Effective extinction coefficient $\beta_\lambda^{e-\mu p}$ spectra of five graphite microparticle populations of identical volume fractions ($f^{\mu p} = 1‰$) differing only by the microparticle uniform diameter $d^{\mu p}$ (100 nm, 300 nm, 1 μm, 3 μm, and 10 μm). The five $\beta_\lambda^{e-\mu p}$ spectra are plotted *versus* the size parameters $x_\lambda^{\mu p} = \pi d^{\mu p}/\lambda$. Each spectrum contains a circle indicating the point $\left(x_\lambda^{\mu p}; \beta_\lambda^{e-\mu p}\right)$ where the wavelength λ is 4 μm. Arrow on the figure indicates increasing values of $d^{\mu p}$.

we have positioned a circle indicating the location of the tracked wavelength of 4 μm, and these five circles clearly reveal the existence of an optimum graphite microparticle diameter producing a maximum effective extinction coefficient $\beta_\lambda^{e-\mu p}$ at $\lambda = 4\,\mu$m: this optimum diameter is probably such that its related size parameter at $\lambda = 4\,\mu$m is equal to one.

The squares and the dashed curve of Fig. 13 show the evolution as a function of the microparticle diameter $d^{\mu p}$ of the radiation thermal conductivity $k^R(T)$ at $T = 300$ K of an NSM consisting of a a-SiO_2 nanoparticle population ($d^{np} = 10$ nm and $f^{np} = 10\%$) and of a graphite microparticle population ($f^{\mu p} = 1‰$) ($k^R(T)$ values on the right scale). When the diameter $d^{\mu p}$ is very small compared to IR wavelengths, the size parameters are very small compared to one, and virtually no scattering is produced by the microparticle population. The level of radiation thermal conductivity $k^R(T)$ is then dictated by the absorption phenomenon only, and is independent of the microparticle diameter $d^{\mu p}$. Let us note here the extraordinarily high absorption efficiency of the graphite particles: very small (10 nm or less in size) and added to the nanoporous a-SiO_2 matrix with a volume fraction as small as 1‰, they result in a decrease

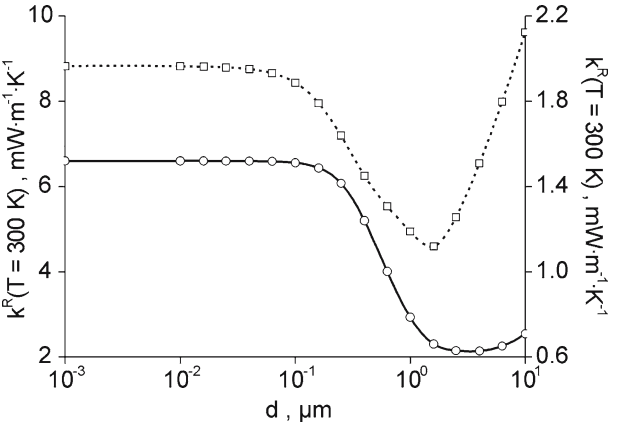

Fig. 13. Dependence of the radiation thermal conductivity $k^R(T)$ of an NSM (at $T = 300\,\mathrm{K}$) as a function of the microparticle population diameter $d^{\mu\mathrm{p}}$. Circles and solid curve refer to an NSM made of a-SiO_2 nanoparticle population ($d^{\mathrm{np}} = 10\,\mathrm{nm}$ and $f^{\mathrm{np}} = 10\%$) and of a a-SiO_2 microparticle population ($f^{\mu\mathrm{p}} = 1‰$) ($k^R(T)$ values on the left scale). Squares and dashed curve refer to an NSM made of the same a-SiO_2 nanoparticle population and of a graphite microparticle population with an unchanged volume fraction ($f^{\mu\mathrm{p}} = 1‰$) ($k^R(T)$ values on the right scale). Circles and squares correspond to values produced by our model, and solid and dashed curves are fits of these two series of data.

in the radiation thermal conductivity of the ensemble by a factor of three (we recall that the radiation thermal conductivity of the nanoporous a-SiO_2 matrix is approximately $6.6\,\mathrm{mW\cdot m^{-1}\cdot K^{-1}}$ at room temperature). Increasing the diameter $d^{\mu\mathrm{p}}$, one reaches a certain threshold (of approximately 100 nm) beyond which the scattering phenomenon starts to contribute consequently to the extinction process. It follows that the radiation thermal conductivity $k^R(T)$ starts to decrease steadily until it reaches a minimum value when the scattering phenomenon operates exactly over the main transparent spectral band (located around $\lambda = 4\,\mu\mathrm{m}$) of the nanoporous a-$SiO_2$ matrix. The optimum microparticle diameter introduced above is thus quite apparent on the graph of Fig. 13; the choice of this particular diameter for the graphite microparticle population can lead to a decrease in the radiation thermal conductivity of the NSM by a factor of almost two. Finally, the value of the optimum microparticle diameter can be estimated from Fig. 13 to be approximately $1.6\,\mu\mathrm{m}$. This value is in fairly good agreement with the one ($1.3\,\mu\mathrm{m}$) expected from the "$x_\lambda^{\mu\mathrm{p}} = \pi d^{\mu\mathrm{p}}/\lambda = 1$ at $\lambda = 4\,\mu\mathrm{m}$" criterion stated above.

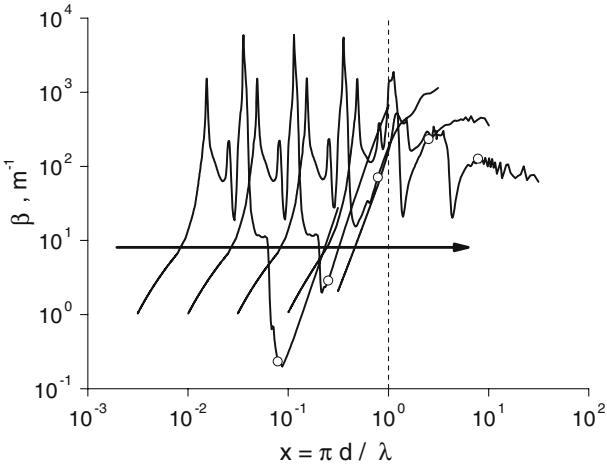

Fig. 14. Effective extinction coefficient $\beta_\lambda^{e-\mu p}$ spectra of five a-SiO_2 microparticle populations of identical volume fractions ($f^{\mu p} = 1‰$) differing only by the microparticle uniform diameter $d^{\mu p}$ (100 nm, 300 nm, 1 μm, 3 μm, and 10 μm). The five $\beta_\lambda^{e-\mu p}$ spectra are plotted *versus* the size parameters $x_\lambda^{\mu p} = \pi d^{\mu p}/\lambda$. Each spectrum contains a circle indicating the point $\left(x_\lambda^{\mu p}; \beta_\lambda^{e-\mu p}\right)$ where the wavelength λ is 4 μm. Arrow on the figure indicates increasing values of $d^{\mu p}$.

For the case of a microparticle population made of a-SiO_2, things are more difficult to analyze because of the complex shape of the extinction index spectrum of the material. The equivalent of Fig. 12 applied to a-SiO_2 microparticle populations yields the graph of Fig. 14: this graph is not as easy to read as the one of Fig. 12, but at least it clearly indicates, through the five circles located on the five $\beta_\lambda^{e-\mu p}$ spectra at the parameter sizes where the wavelength λ is 4 μm, that once again an optimum microparticle diameter exists, located around the value of 3 μm, for which the extinction produced by the a-SiO_2 microparticle population – exclusively through the scattering phenomenon – hits the $\lambda \approx 4\,\mu$m IR zone in the most efficient way. This point is corroborated by the circles and the solid curve of Fig. 13, which show the evolution as a function of the microparticle diameter $d^{\mu p}$ of the radiation thermal conductivity $k^R(T)$ at $T = 300$ K of an NSM made of a a-SiO_2 nanoparticle population ($d^{np} = 10$ nm and $f^{np} = 10\%$) and of a a-SiO_2 microparticle population ($f^{\mu p} = 1‰$) ($k^R(T)$ values on the left scale). For very small values of the microparticle diameter $d^{\mu p}$, neither scattering nor absorption is produced by the a-SiO_2 microparticle population, so that the radiation thermal conductivity

$k^R(T)$ of the NSM is equal to that of the nanoporous a-SiO_2 matrix ($6.6\ \mathrm{mW \cdot m^{-1} \cdot K^{-1}}$). The optimum diameter for the a-SiO_2 microparticle population (corresponding to an optimum spectral localization of the scattering phenomenon) is around $3\,\mu$m, and the choice of this particular microparticle diameter leads to a decrease in the radiation thermal conductivity of the NSM by a factor of three.

7. SUMMARY AND PERSPECTIVES

In the first part of this contribution, we have presented a model for the evaluation of the radiation heat transfer traveling through NSMs in relation with the compositions (sizes, volume fractions, and physical nature of the different populations of constituents) of these materials. Our model is very rudimentary; it relies on the Rosseland diffusion approximation and the related notion of radiation thermal conductivity. Nevertheless, we have extended the field of application of this theory in order to integrate spectral dependences of the radiative properties of the constituents as well as anisotropic scattering effects in our calculations. Besides, the notion of radiation thermal conductivity being based on the concepts of refractive index and effective extinction coefficient spectra, we have detailed the principles of the optical and radiative homogenization techniques that we employ for the determination of these two spectra for the case of an NSM of known composition.

In the second part of this paper, we have used our model (i) to get a better understanding of the different radiative transfer phenomena that take place within NSMs, and (ii) if possible, to derive guidelines towards enhanced radiative insulation efficiencies of these materials. First, we have demonstrated that a nanoporous a-SiO_2 matrix presents an unacceptable transparent behavior over a narrow spectral band located around $4\,\mu$m, and we have deduced that an efficient microparticle population, i.e., a microparticle population able to cut down the radiation thermal conductivity of the matrix, must provide a strong extinction over this transparent spectral domain. Then, in order to decorrelate the scattering and absorption phenomena in the extinction process, we have selected, for the constitution of the microparticle populations, two materials presenting extremely different optical properties around the tracked wavelength of $4\,\mu$m: on the one hand, a-SiO_2, very transparent, and on the other hand, graphite, very opaque. The different series of calculations that we have performed on the two NSMs described above (the first NSM being made of a nanoporous a-SiO_2 matrix and of a a-SiO_2 microparticle population, and the second NSM being made of the same nanoporous a-SiO_2 matrix and of a graphite microparticle population) have

brought us to the following conclusions: (i) whatever the material constituting the microparticle population, provided the average diameter $d^{\mu p}$ of this population is of the right order of magnitude (see below), the presence of the microparticle population within the nanoporous a-SiO_2 matrix contributes to an efficient drop in the radiation thermal conductivity of the NSM; (ii) if the material constituting the microparticle population is transparent around $4\,\mu$m, extinction is produced by the microparticles exclusively *via* the scattering phenomenon; (iii) if, on the other hand, the material is opaque around $4\,\mu$m, both scattering and absorption contribute to the extinction process, resulting in an optimized efficiency of the microparticle population in terms of opacity production; (iv) the scattering phenomenon from a microparticle population of uniform diameter $d^{\mu p}$ impacting the spectral domain around a wavelength λ given by $\pi d^{\mu p}/\lambda \approx 1$, it follows that the diameter $d^{\mu p}$ of the microparticles must be of the order of $1\,\mu$m (in order for the scattering phenomenon to track the $\lambda \approx 4\,\mu$m wavelengths) and that an optimum diameter $d^{\mu p}$ exists for which the scattering process hits the $\lambda \approx 4\,\mu$m IR zone in the most efficient way; (v) finally, the radiation thermal conductivity of an NSM decreases considerably as soon as a volume fraction as small as $1‰$ of the microparticle population is inserted into the material. All these conclusions will be exploited in the near future: they should guide us towards the formulation of new NSMs with optimized radiative properties.

Obviously, the modeling strategy that we have chosen is extremely basic. Investigation of the radiation heat transfer and of the interaction of this radiation mode with the conduction mode within nanoporous superinsulating materials is actually a vast research subject involving numerous activities in various fields such as radiative homogenization, coupled radiation and conduction heat transfer within semitransparent materials and thermal characterization. As far as heat transfer modeling is concerned, we will concentrate in the future on several studies related to the radiative homogenization theme: (i) impact of the nanometric scale of the a-SiO_2 particles on the features of their dielectric permittivity function (the phonons within such tiny particles having a quasi-ballistic behavior); (ii) effect of a non-uniform distribution of the a-SiO_2 nanoparticle diameters on the effective radiative properties of the nanoporous a-SiO_2 matrix (during the fabrication process, the a-SiO_2 nanoparticles coalesce to one another and form agglomerates the sizes of which can reach several hundreds of nm); (iii) deeper analysis of the dependent nature of the scattering phenomenon, especially within the nanoporous a-SiO_2 matrix; and (iv) finally, integration of the fibers in the radiative homogenization procedure.

REFERENCES

1. H. M. Strong, F. P. Bundy, and H. P. Bovenkerk, *J. Appl. Phys.* **31**:39 (1960).
2. H. Bjurström, E. Karawacki, and B. Carlsson, *Int. J. Heat Mass Transfer* **27**:2025 (1984).
3. D. W. Yarbrough, T. W. Tong, and D. L. McElroy, *High Temp. Sci.* **19**:213 (1985).
4. P. Scheuerpflug, R. Caps, D. Buttner, and J. Fricke, *Int. J. Heat Mass Transfer* **28**:2299 (1985).
5. C. Stark and J. Fricke, *Int. J. Heat Mass Transfer* **36**:617 (1993).
6. M. F. Modest, *Radiative Heat Transfer* (McGraw-Hill, New York, 1993).
7. C. M. Chu and S. W. Churchill, *Trans. Antennas Propagation* **AP-4**:142 (1956).
8. C. F. Bohren and D. R. Huffman, *Absorption and Scattering of Light by Small Particles* (Wiley, New York, 1983).
9. Optical properties of a-SiO_2: *Handbook of Optical Constants of Solids*, E. D. Palik, ed. (Academic Press, San Diego, 1985); optical properties of graphite: *Handbook of Optical Constants of Solids II*, E. D. Palik, ed. (Academic Press, San Diego, 1991).
10. M. Kaviany *Principles of Heat Transfer in Porous Media*. 2nd Ed. (Springer, New York, 1995).
11. H. S. Chu, A. J. Stretton, and C. L. Tien, *Int. J. Heat Mass Transfer* **31**:1627 (1988).